RSC Advances

ROYAL SOCIETY OF CHEMISTRY

www.rsc.org/advances

Journal Name

ARTICLE

Phthalazinone Structure-Based Covalent Triazine Frameworks and Their Gas Adsorption and Separation Properties

Received 00th January 20xx,
Accepted 00th January 20xx

DOI: 10.1039/x0xx00000x

www.rsc.org/

Kuanyu Yuan,[a] Cheng Liu,*[a] Jianhua Han,[a] Guipeng Yu,[b] Jinyan Wang,[a] Hongmin Duan,[c] Zhonggang Wang,[a] and Xigao Jian[a]

In this work, the new classes of phthalazinone-based covalent triazine frameworks (PHCTFs) were prepared by ionothermal synthesis from two full rigid dicyano building blocks with rigid, thermostable and asymmetric *N*-heterocycle-containing structure. The surface and internal morphologies of PHCTFs were examined by FE-SEM and TEM. The resultant microporous polymers, PHCTFs, exhibited BET specific surface area up to 1845 $m^2 g^{-1}$ and moderately narrow pore size distribution. According to the sorption measurements, the CO_2 uptake can be up to 17.1 wt% (273 K/1 bar) and the H_2 uptake can be up to 1.92 wt% (77 K/1 bar). Moreover, the initial slopes of the single component gas adsorption isotherms in the low pressure range were used as the gas separation ratios. The obtained polymer networks possess satisfactory CO_2/N_2 selectivity performance up to 52 and CO_2/CH_4 selectivity up to 12. Combining the relationship of the structure and performance, it can be concluded that the twisted and non-coplanar topology conformation can be used to improve the porosity of the microporous organic polymers. At the same time, the nitrogen- and oxygen-rich characteristics of phthalazinone core endow the networks strong affinity for CO_2 and thereby high CO_2 adsorption capacity. So the pore structure and chemical composition may play very important role on the adsorption properties of small gas molecules.

Introduction

The porous materials including macroporous (>50 nm), mesoporous (2-50 nm) and microporous (<2 nm) materials are classified by IUPAC according to their pore size[1]. For their special porous architectures, micro- and nanoscale range, these materials have attracted much attention in many fields of science and technology, especially in advanced functional material design[2]. Apart from traditional types of porous materials, such as activated carbon, zeolites[3], or mesoporous silicates[4], metal-organic frameworks[5] (MOFs) containing larger organic linkers and metal ions have been one of the fastest growing fields in chemistry during the past decades for their high surface areas and large range levels of porosity. However, the low polysicochemical stability of MOFs may limit their widely applications[6].

In the past few years, purely microporous organic polymers (MOPs) materials, which are constructed through strong covalent bonding via polymerization of building blocks that composed of non-metallic elements such as C, H, O, N and B[7], have attracted much considerable attention. The relatively high surface area, permanent porosity, low mass densities and wide structure turnability[8] make MOPs show great potential in gas storage[9] and separation[10], catalysis[11] and sensors[12]. Several different classes of MOPs have been developed, including covalent organic frameworks (COFs)[13], conjugated microporous polymers (CMPs)[14], porous aromatic frameworks (PAFs)[15], porous polymer networks (PPNs)[16], polymers of intrinsic microporosity (PIMs)[17], hypercrosslinked polymers (HCPs)[9a, 18], element-organic frameworks (EOFs)[11b, 19] and organic cage frameworks (OCFs)[20]. In consequence of the remarkably potential application of MOPs, exploiting new structure or new performance remains a research hot issue in this field.

Due to the plethora of organic reactions and building blocks[17b, 21], which provide flexibility for the materials to be designed to achieve desirable pore properties[22], various reactions[7b] of organic functional groups make contribution to the construction of MOPs, such as reversible borate chemistry, palladium–catalyzed Sonogashira–Hagihara cross-coupling, homocoupling of aromatic bromides, Friedel-Crafts reaction, dioxane-forming polymerization, oxidative coupling, amide or imide formation and Schiff-base chemistry. Recently, an emerging class of microporous organic materials called covalent triazine frameworks[23] (CTFs), which own the novel polymer network based on triazine linkage through the trimerization of nitriles, provides a new method to construct the MOPs.

[a] State Key Laboratory of Fine Chemicals, Department of Polymer Science and Materials, School of Chemical Engineering, Dalian University of Technology, Dalian, People's Republic of China, 116024. E-mail: liuch1115@dlut.edu.cn
Department of Polymer Materials & Engineering, Dalian University of Technology, Dalian, People's Republic of China, 116024
Liaoning Province Engineering Research Centre of High Performance Resins, Dalian, People's Republic of China, 116024
[b] College of Chemistry and Chemical Engineering, Central South University, Changsha, People's Republic of China, 410083.
[c] Dalian Institute of Chemical Physics, Chinese Academy of Science, Dalian, People's Republic of China, 116023.

Electronic Supplementary Information (ESI) available: This section contains ten figures, including the TGA curves of aromatic cyanide monomers and PHCTFs, ^{1}H-NMR spectra of aromatic cyanide monomers, XRD patterns, elemental analysis and adsorption selectivity of CO_2 over CH_4 and N_2 at 273 and 298 K of PHCTFs. See DOI: 10.1039/x0xx00000x

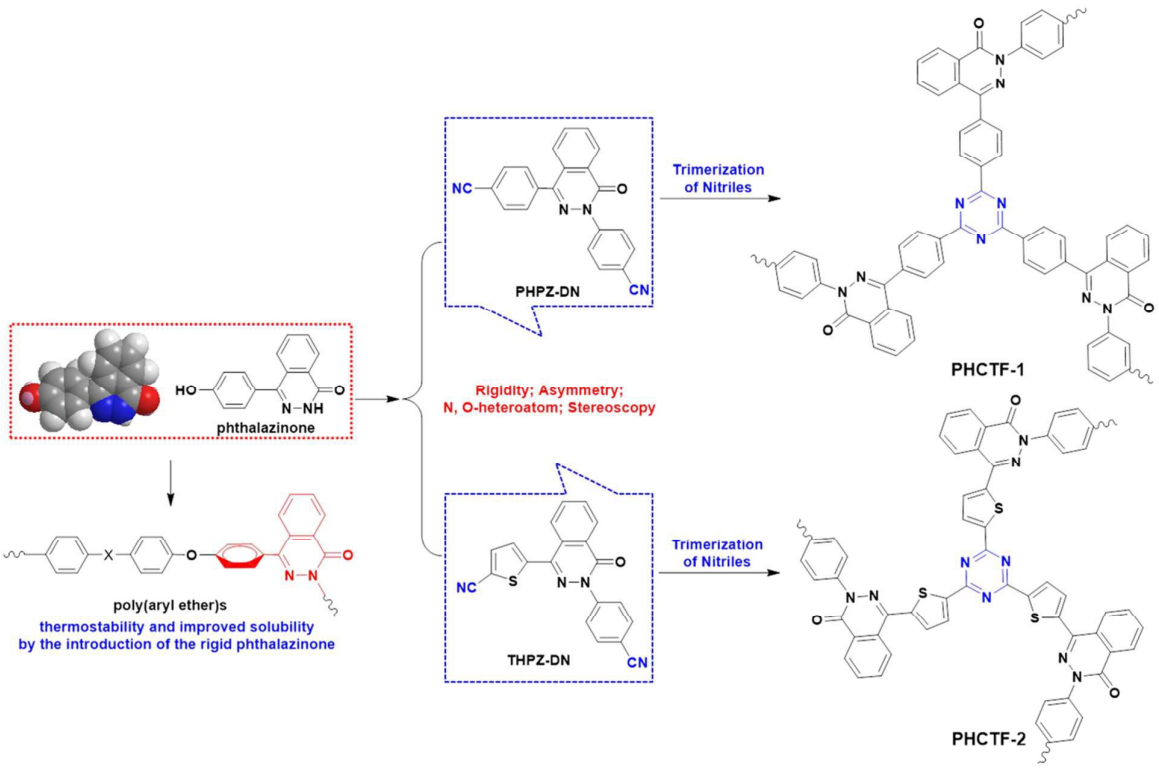

Scheme 1. Synthetic route of phthalazinone core-based covalent triazine frameworks-PHCTFs.

Covalent triazine frameworks (CTFs) were first developed by Antonietti, Thomas and co-workers via ionothermal synthesis[23d] in Zinc chloride ($ZnCl_2$) salt melts medium in 2008. Though, the reaction was performed at high temperature (400-700 ^oC) for long time and may deteriorate the structure of some monomers as well as carbonize the derived polymers[24]. In 2012, Zhu and co-authors[25] reported an alternative method which used strong bronsted acid-trifluoromethanesulfonic acid to catalyze the cyclotrimerization reaction at mild conditions. Compared with the latter, however, the ionthermal method shows such significant advantages[26] as being cheaper and experimentally simpler, and yielding materials with high surface areas.

Apart from the specialty of the synthesis of CTFs, they possess very large specific surface area together with[27] exceptional chemical inertness and high thermal stability owing to their graphite-like composition and robust carbon–carbon and carbon–nitrogen linkages.

The large specific surface areas of CTFs can be ascribed to the abundant pore structure, primarily micropores and mesopores. And the micropores, especially the narrow ultramicropores (< 1nm), make greater contribution to the gas molecules, such as the small thermodynamic size gas molecule CO_2. Also, the incorporation of the nitrogen-rich polar triazine moieties makes CTFs electron-rich, which may enhance the affinity and the isosteric heat between the adsorbent and specific sorbate molecule by the significantly promoted dipole-quadrupole interaction[28]. The co-contribution of above factors, microporoes and nitrogen-rich, enables CTFs material to be a promising candidate for gas adsorption and separation. Meanwhile, CTFs with *N*-doping show potential catalysts supporter by nitrogen-metal interactions in large amounts owing to the large accessible surface areas[27]. All of the characterizes and advantages in structure and functionality make CTFs be considered as a promising candidate for energy gas storage and catalytic support materials, and have spurred the scientific interest in searching novel building blocks to construct versatile CTFs.

Motivated by the above-mentioned distinctions and advantages of CTFs, we wonder the effect of *N*-heterocycle-containing, rigid, twisted and asymmetric structure on the properties of CTFs. We have previously demonstrated the synthesis and properties of aromatic polymers containing phthalazinone moiety[29], such as poly(aryl ether)s[30], polyamides[31], polyimides[32], and so on, which possess rigid and twisted backbones and remain excellent thermostability coupled with improved solubility due to the introduction of the rigid phthalazinone with twisted, non-coplanar conformation. Therefore, we consider that this stereoscopic phthalazinone core, which favors the construction of CTFs and limits the stacking of the polymers networks, may help to increase the available space accessible for gas adsorption and storage. To the best of our knowledge, there are no same building blocks, which simultaneously possess rigidity, asymmetry, *N, O*-heteroatoms and stereoscopy, have been selected to construct CTFs.

In our work, we designed and synthesized two fully rigid dicyano building blocks containing phthalazinone structure, 2-(4'-cyanophenyl)-4-(4'-cyanophenyl)-2,3-phthalazin-1-one (PHPZ-DN) and 2-(4'-cyanophenyl)-4-(4'-cyanothiophene)-2,3-phthalazin-1-one (THPZ-DN). Then, new classes of phthalazinone core-based covalent triazine frameworks (PHCTFs) (Scheme 1) were prepared by ionothermal reaction and their porosity, gas storage capacities and selectivity have also been characterized by different pure gas adsorption/desorption measurements. The conformation of THPZ-DN exhibits more coplanarity, because the dihedral angle calculated by Gaussian 09W between thiophene and naphthyridine of THPZ-DN is smaller than phenyl and naphthyridine of PHPZ-DN. This is another aim to demonstrate how the change of conformation of phthalazinone influences the porosity of the targeted polymer networks.

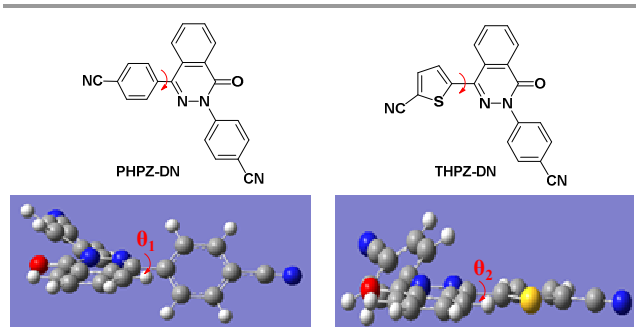

Figure 1. The dihedral angle (θ) calculated by Gaussian 09w by energy-minimized conformation.

Experimental

Material

All the starting materials were purchased from commercial suppliers and used as received unless otherwise indicated. Zinc chloride was refluxed and distilled over thionyl chloride to remove water, and then excess thionyl chloride was azeotropically distilled with toluene. After the removal of thionyl chloride and toluene, anhydrous zinc chloride was obtained after being dried at 180 °C under vacuum for 24 h.

Instrumentation

Fourier transform infrared spectra (FT-IR) were recorded using a Nicolet 20 DXB FT-IR spectrophotometer in the 400–4000 cm^{-1} region. Samples were prepared by dispersing the complexes in potassium bromide (KBr) and compressing the mixtures to form disks. ^{1}H-NMR (400 Hz) spectra were obtained with a Brucker spectrometer at an operating temperature of 25 ^oC using tetramethylsilane as an internal standard. Elemental analyses were determined with an Elementar Vario EL III elemental analyzer. Thermogravimetric analysis (TGA) of the polymers was performed on a Mettler TGA/SDTA851 thermogravimetric analysis instrument in flowing nitrogen atmosphere at a heating rate 20 ^oC/min. The temperature range was from room temperature to 800 °C. The powder X-ray diffraction patterns (XRD) of the samples were recorded with a SmartLab (9) diffractometer using CuKα radiation operated at 45 kV and 200 mA, performing from 5° to 80° at a speed of 8°·min^{-1}. Field-emission scanning electron microscopy (FE-SEM) experiments were carried on a Nova NanoSEM 450. Transmission electron microscopy (TEM) images were carried out using Tecnai12 transmission electron microscopy (FEI, Eindhoven, The Netherlands) at an operating voltage of 120 kV. Adsorption and desorption measurements for all the gases were conducted on an Autosorb iQ (Quantachrome) analyzer. Before sorption measurements, the samples were degassed at 120 °C under high vacuum for 12 h. The nitrogen adsorption and desorption were measured at 77 and 273 K up to 1 bar. The specific surface areas were calculated according to the Brunauer–Emmett–Teller (BET) model in the relative pressure (P/P_0) ranging from 0.01 to 0.1. Pore size distributions were derived from the N_2 adsorption isotherms at 77 K using the nonlocal density functional theory (NLDFT) method. High-purity gas (99.999%) was used for adsorption experiment.

Synthesis of 2-(4-cyanophenyl)-4-(4-bromophenyl)(2H)phthalazin-1-one (PHPZ-CN).

A 250-mL three-necked round-bottom flask equipped with a mechanical stirrer, a Dean-Stark trap outfitted with a condenser, and nitrogen inlet and outlet, was charged with 1,2-dihydro-4-(4-bromophenyl)(2H)phthalazin-1-one (PHPZ-Br) (9.03 g, 0.03 mol), potassium carbonate (K_2CO_3, 2.82 g, 0.02 mol), *N*,*N*-dimethylacetamide (DMAc, 60 mL) and toluene (50 mL). Under an atmosphere of nitrogen, the reaction mixture was heated and maintained at 140 ^oC for 4-5 h to remove all water by means of azeotropic distillation with toluene. Then, the temperature was increased to 150 ^oC to remove toluene for 4 h. After the mixture was cooled to room temperature, 4.95 g (0.04 mol) of 4-chlorobenzonitrile was added and the temperature was maintained at 180 ^oC for 8 h. The mixture was then poured into an ethanol/water mixture (1 : 1 (v/v), 200 mL). The precipitate was collected on a filter and crystallized from *N*,*N*-dimethylformamide (DMF) to give white solid (10.15 g, yield: 84%), mp: 278-279 ^oC; ^{1}H-NMR (400 MHz, DMSO-d_6/TMS int, ppm) δ: 8.47 (d, 1H), 8.03-7.96 (m, 6H), 7.82-7.74 (m, 3H), 7.67 (d, 2H); HRMS calculated for $C_{21}H_{12}BrN_3O$, 401.0164; found, 401.0159.

Synthesis of 2-(4'-cyanophenyl)-4-(4'-cyanophenyl)(2H)phthalazin-1-one (PHPZ-DN).

A 250-mL three-necked round-bottom flask equipped with a magnetic stirrer a condenser was charged with PHPZ-CN (7.240 g, 0.018 mol), potassium hexacyanoferrate ($K_4[Fe(CN)_6]\cdot 3H_2O$, 1.673 g, 0.004 mol, 0.22 equiv), sodium carbonate (Na_2CO_3, 1.908 g, 0.018 mol, 1.0 equiv), palladium acetate ($Pd(OAc)_2$, 0.020g, 0.5%), and 1-methyl-2-pyrrolidinone (NMP, 100 mL). The flask was evacuated and filled with nitrogen (two times) and heated to 140 ^oC. After maintaining the temperature for 12 h, the reaction mixture was then poured into diluted water. The precipitate was collected on the filter and crystallized from DMAc and dimethyl sulfoxide (DMSO) to give white solid (3.564 g, 57%), mp: 312-313 ^oC; ^{1}H-NMR (400 MHz, $CDCl_3$/TMS int, ppm) δ: 8.64 (d, 1H), 7.98 (d, 2H), 7.88 (d, 4H), 7.78 (d, 4H), 7.71 (d, 1H); HRMS calculated for $C_{22}H_{12}N_4O$, 348.1011; found, 348.1020.

Synthesis of 2-(4'-cyanophenyl)-4-(4'-bromothiophene)-2,3-phthalazin-1-one (THPZ-CN).

A 250-mL three-necked round-bottom flask equipped with a mechanical stirrer, nitrogen inlet and outlet and a condenser was charged with 1,2-dihydro-4-(4-bromothiophene)(2H)phthalazin-1-one (THPZ) (9.22 g, 0.03 mol), cesium fluoride (CsF, 5.47 g, 0.036 mol), 4-fluorobenzonitrile (4.36 g, 0.036 mol) and DMAc (30 mL). Under the N_2 atmosphere, the reaction mixture was heated and maintained at 150 °C for 12 h. Then, the mixture was poured into an ethanol/water mixture (1 : 1, 200 mL). The precipitate was collected on a filter and crystallized from DMF to give yellow solid (10.42 g, 85%); m.p: 258-259 °C; ^{1}H-NMR (400 MHz, DMSO-d_6/TMS int, ppm) δ: 8.43-8.49 (d, 1H), 8.22-8.27 (d, 1H), 7.92-8.10 (m, 6H), 7.58-7.62 (d, 1H), 7.39-7.43 (d, 1H). HRMS calculated for $C_{19}H_{10}BrN_3OS$: 406.9728; found: 406.9723.

Synthesis of 2-(4'-cyanothiophene)-4-(4'-cyanophenyl)(2H)phthalazin-1-one(THPZ-DN)

THPZ-CN (4.08 g, 10 mmol), cuprous cyanide (CuCN, 4.48 g, 50 mmol) and 18-crown-6 (90 mg) were dissolved in dry DMF (100 mL) under N_2 atmosphere. After stirred at 150 °C for 24 h, the mixture was poured into a cold dilute ammonia water and stirred for 12 h. The brown solid was collected by filtration, washed with water and ethanol several times, dried under vacuum and crystallized from DMF to give a light brown solid (2.32 g, 66%); m.p: 270-271°C. ^{1}H-NMR (400 MHz, DMSO-d_6/TMS int, ppm) δ: 8.44-8.50 (d, 1H), 8.17-8.22 (d, 1H), 7.94-8.10 (m, 6H), 7.88-7.91 (d, 1H). HRMS calculated for $C_{20}H_{10}N_4OS$: 354.0575; found: 354.0569.

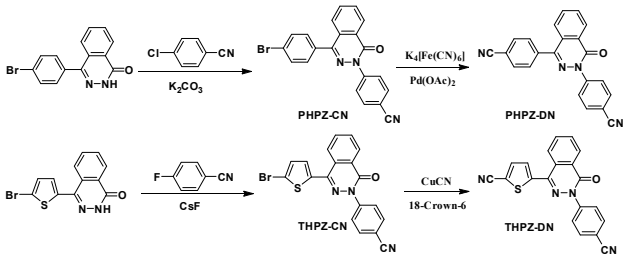

Scheme 2. Synthetic routes of phthalazinone-based monomers, PHPZ-DN and THPZ-DN.

Synthesis of PHCTFs

PHCTFs were synthesized by heating a mixture of the resultant phthalazinone-based monomers, PHPZ-DN or THPZ-DN, with $ZnCl_2$ (Table 1). The two kinds of PHCTFs were synthesized by a similar method, so only the synthesis procedure for PHCTF-1a is afforded here as an example. A quartz tube (3 × 5 cm) was charged with PHPZ-DN (0.16 g, 0.45 mmol) and $ZnCl_2$ (0.61 g, 4.5 mmol). The tube was evacuated to a high vacuum and then sealed rapidly. After a temperature program (250 °C for 10 h, 300 °C for 10 h, 350 °C for 10 h, and 400 °C for 20 h), the quartz tube was cooled to room temperature, and the resultant mixture was subsequently ground and then washed thoroughly with water for 72 h to remove most of the catalyst. After that, the product was isolated by filtration and again stirred with 100 mL hydrochloric acid (HCl, 2 mol/L) for 24 h to remove the residual salt. The resulting black powder was filtered and washed successively with water and alcohol, followed by an overnight Soxhlet extraction using acetone and methyl alcohol as eluting solvents sequentially, and finally dried in vacuum at 150 °C. Yield: 80%.

Table 1. Synthesis of PHCTFs.

PHCTF	Monomer : $ZnCl_2$ (molar ratio)	Temperature (°C)/(Time)
1a	1:10	250(10h), 300(10h), 350(10h), 400(20h)
1b	1:5	250(10h), 300(10h), 350(10h), 400(20h)
1c	1:10	250(10h), 300(10h), 350(10h), 400(20h), 600(20h)
2a	1:10	250(10h), 300(10h), 350(10h), 400(20h)
2b	1:5	250(10h), 300(10h), 350(10h), 400(20h)

Results and discussion

Two analogous phthalazinone-containing dicyano monomers were selected as building blocks, which were synthesized by nucleophilic substitution reaction, followed by cyanation (the PHPZ-DN was prepared from the cyanation of PHPZ-Br according to the procedure of literature[33] with some modifications). The synthetic routes are illustrated in Scheme 2 and their proposed structures were confirmed by ^{1}H-NMR (Figure S1 and Figure S2 of the Supporting Information). Although using strong Brønsted acid as catalyst, trifluoromethanesulfonic acid etc, may avoid decomposition and condensation reactions such as C-H bond cleavage and carbonization[34], this method generally leads to lower surface areas accompanied with the breakage within C-N and C-O linkage of the nitrile monomers[35]. In contrast, CTFs constructed from 1,4-dicyanobenene at the presence of $ZnCl_2$ as Lewis acid catalyst, solvent and porogen, exhibited high surface areas (1710 m^2 g^{-1} to 3000 m^2 g^{-1})[23a, 23c], but the dicyano monomer should suffer continuous heating at 400 °C or even higher temperature (600 °C) during the reaction. The relative excellent thermostability (Figure S3) of the building blocks seems to also be necessary to afford complete and good physicochemical stabile polymer networks. The 10% decomposition temperatures under N_2 atmosphere recorded at 336 °C for PHPZ-DN and 364 °C for THPZ-DN may be a little lower compared to previous reported dicyano monomers, o-DCB and DCBP[23d] (the temperatures for 10 wt% mass loss under N_2

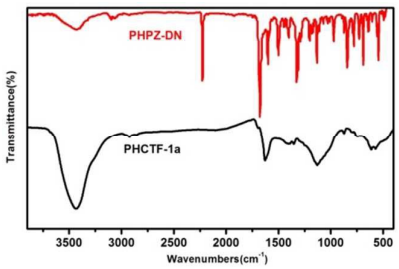

Figure 2. FT-IR spectra of PHPZ-DN and PHCTF1a.

atmosphere exceed 400 °C), so the trimerization reaction was conducted under a high vacuum system to avoid the rapid decomposition under high temperature and long reaction time.

According to Yu's research [35], the reaction temperature less than 350 °C results in low-molecular-weight compounds. So, to avoid the probable complete carbonization by the one-step procedure to high polymerization temperature, the stepwise heating procedure[35] was applied to prepare the powdered PHCTFs successfully in good yield (Scheme 1). The obtained materials, PHCTFs, are insoluble in any common organic solvents, such as DMSO, NMP and tetrahydrofuran (THF), implying good chemical stability. The formation of PHCTFs frameworks was confirmed by Fourier transform infrared (FT-IR). Notably, taking PHCTF-1a for example (Figure 2), the strong intense characteristic C ≡ N stretching band of the building block (PHPZ-DN) around 2238 cm^{-1} disappeared, as well as the formation the new characteristic C-N stretching bands for triazine at 1352 cm^{-1} and 1497 cm^{-1} (Figure 2).

As indicated by the X-ray diffraction (XRD) measurements (Figure S4), they are amorphous and have less structural order as most reported CTFs materials[26-27]. The variations of the of contents of *N*-heteroatom during high temperature polymerization reaction were detected by elemental analysis (Table S1), giving relative lower nitrogen content and concomitantly an increasing trend in C/N ratio compared with the theoretically calculated values. Referring to related researches[34], an amount of nitrile decomposition involving C-H and Ar-CN elinmination should be taken into account. For the potential broad application of the porous frameworks, the thermal stability of the obtained frameworks should be considered. The thermogravimetric analysis (Figure S5) under nitrogen atmosphere of PHCTFs indicates that the polymer skeleton decomposition starts at 520 °C, suggesting its good thermal stability. Some mass amount before the skeleton decomposition may be attributed to the hydrated water and solvents. Surface morphologies of PHCTFs were evaluated by field-emission scanning electron microscopy (FE-SEM) (Figure 3), showing the similar surface morphology in line with their respective similar porosity characteristics from N_2 sorption studies except PHCTF-1c. The local structure was observed through transmission electron microscopy (TEM) (Figure 3). From the TEM images, various irregular-shaped microparticles can be seen, which are agglomerated and interconnected with a continuous polymeric phase. Such disordered and amorphous structures shown in the TEM imagines are consistent with other amorphous microporous organic polymers[36].

The porosity parameters and surface areas (Figure 4) of the PHCTFs were investigated by nitrogen sorption at 77K, and the pore sizes and distributions were calculated by the nonlocal density functional theory (NLDFT) from their N_2 adsorption-desorption isotherms. The isotherms demonstrated rapid nitrogen uptake and high gas uptake at relative pressure (P/P_0) less than 0.01, indicative of the characteristics of permanent micropores. Figure 4 shows that PHCTFs more or less display

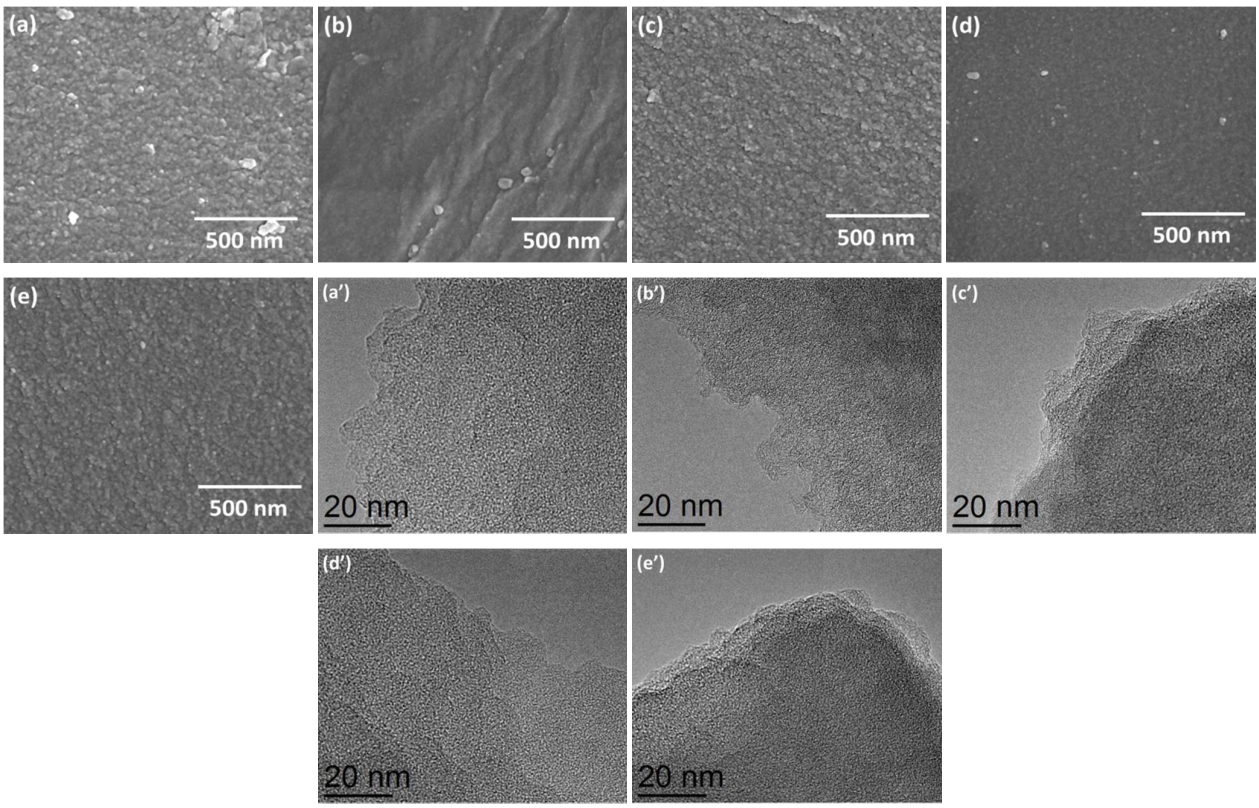

Figure 3. FE-SEM images of (a) PHCTF-1a, (b) PHCTF-1b, (c) PHCTF-1c, (d) PHCTF-2a and (e) PHCTF-2b at 500nm. TEM images of (a') PHCTF-1a, (b') PHCTF-1b, (c') PHCTF-1c, (d') PHCTF-2a and (e') PHCTF-2b.

apparent hysteresis loop, demonstrating the presence of mesopores, especially for PHCTF-1c, which may result from the softness of the organic polymer skeleton and swelling effect should be the dominant reason, resulting in combination of type I and IV characteristics and co-existence of micropores and mesopores of PHCTF-1c. On the one hand, the breakage of the polymer network is more likely to happen because of its organic nature. On the other hand, triazine retrotrimerization should be taken into account and opening triazine cross-links leads to local expansions of the network[23a]. The apparent surface areas calculated from Brunauer-Emmett-Teller (BET) models within the pressure range of P/P_0 = 0.05-0.1 are shown in Table 2. The BET surface areas seem to be associated closely with the polymerization reaction temperature, consequently the highest surface area of PHCTF-1c. A comparison of pore size distribution (PSD) obtained by fitting the nitrogen uptake branch of the isotherms with the non-local density function theory (NLDFT) is illustrated in Figure 4. Although PHCTF polymer networks exhibit amorphous nature, they have relative uniform micropores with a diameter less than 2 nm except for PHCTF-1c, which PHCTF-1c simultaneously possesses micropores centering at 1.3 nm and mesopores at 5.8 nm.

The above results of porosity parameters and surface areas of PHCTFs indicate that the phthalazinone-based building blocks with a rigid, twisted and non-coplanar structure can be used in the fabrication of the MOPs with relatively high surface areas (maximum to 1845 $m^2 g^{-1}$) and narrow pore size distributions. In this study, the two phthalazinone-based building blocks have

Table 2. Porosity data for PHCTFs from N_2 isotherms at 77K.

PHCTF	S_{BET} [a] ($m^2 g^{-1}$)	S_{Lang} [b] ($m^2 g^{-1}$)	V_{micro} [c] ($cm^3 g^{-1}$)	V_{tot} [d] ($cm^3 g^{-1}$)	V_{micro} / V_{tot}
1a	1062	1499	0.44	0.56	0.79
1b	955	1223	0.40	0.46	0.89
1c	1845	3046	0.28	1.32	0.21
2a	731	989	0.20	0.42	0.48
2b	887	1267	0.28	0.52	0.54

[a] Calculated BET surface area over the pressure range 0.05-0.1 P/P_0. [b] Langmuir surface area over the pressure range 0.05-0.3 P/P_0. [c] Micropore volume was calculated using the t-plot method. [d] Total pore volume at P/P_0 = 0.9.

similar structures, but not identical geometry conformation (Figure 1). The dihedral angle (θ_1) of the phenyl ring and naphthyridine of PHPZ-DN is about 48°, which is much larger than the dihedral angle (θ_2) between thiophene and naphthyridine of THPZ-DN. So the steric conformation of PHPZ-DN may theoretically impart much more advantage to increasing inter-chain porosity from the network interpenetrating of polymer network than the approximately plane V-shaped conformation of THPZ-DN. The fact of the higher BET surface areas of PHCTF-1 than that of PHCTF-2, as well as the pore volumes, also reflects this influence trend. This is because the plane V-shaped conformation of THPZ-DN makes the polymer incline to form two-dimensional network resulted from the possible π-π stacking between layers[37]. While the more twisted and non-coplanar conformation of PHPZ-DN is helpful to form the network with more and a little larger

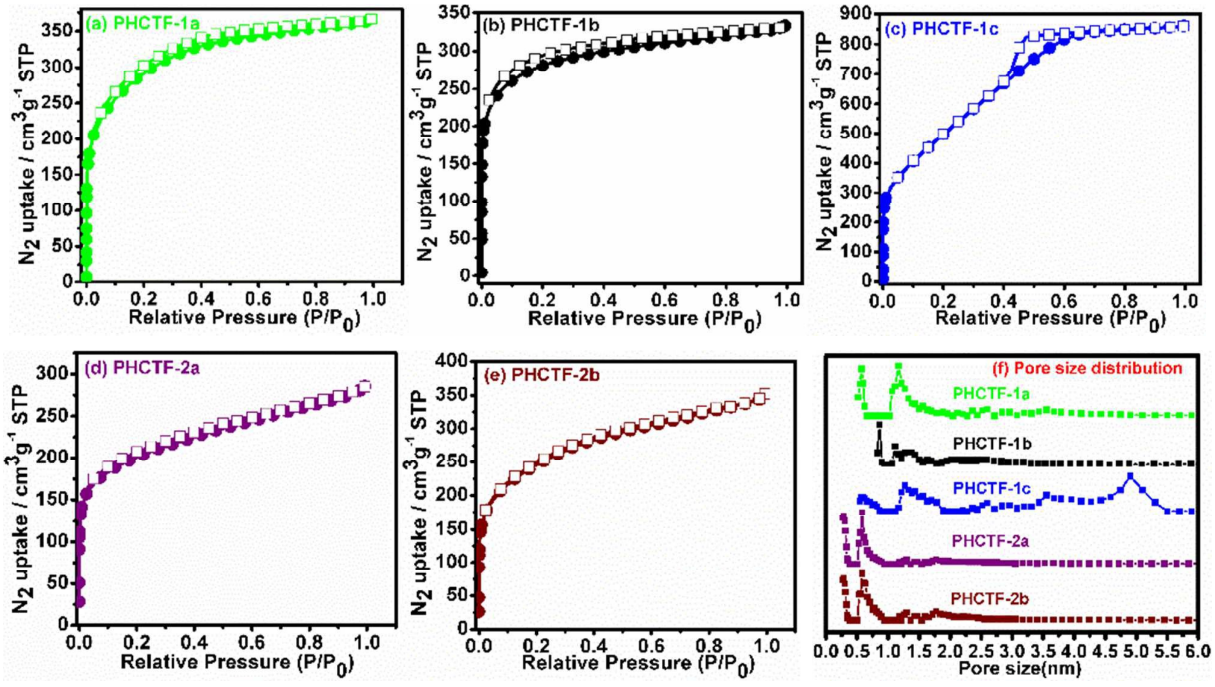

Figure 4. Nitrogen adsorption (filled)-desorption (empty) isotherms and NLDFT pore size distribution (PSD) curves of PHCTFs.

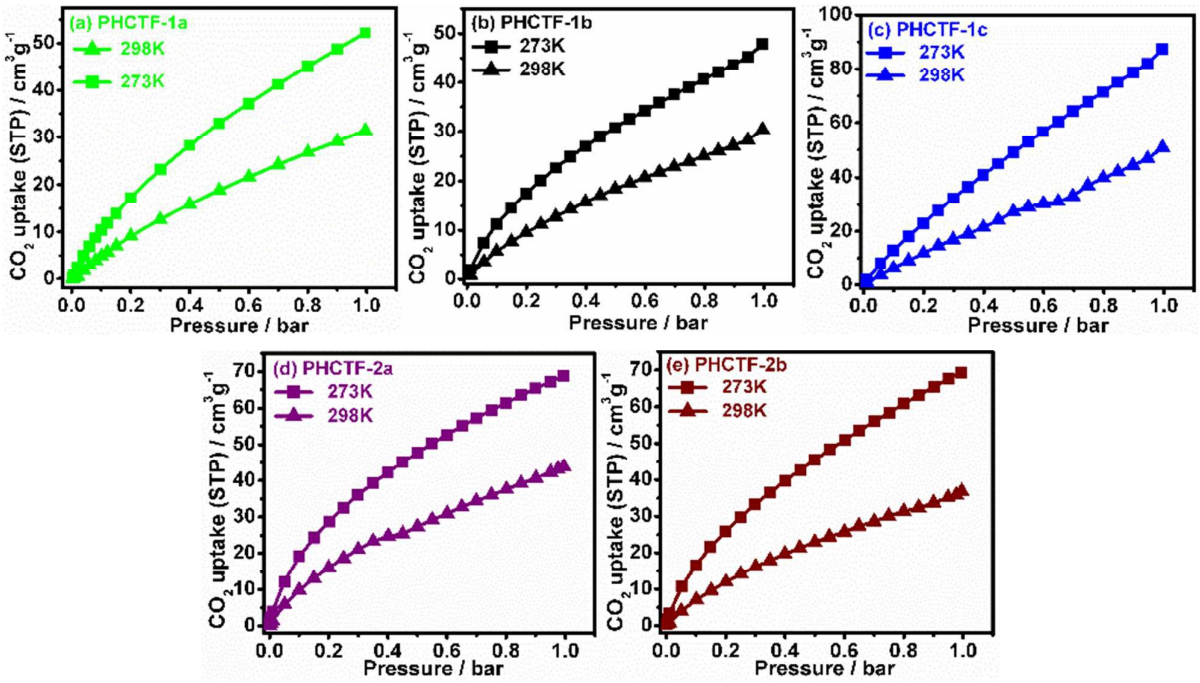

Figure 5. Carbon dioxide adsorption isotherms of the obtained PHCTFs at 273 K and 298 K.

micropores, which results in the increased BET surface areas of it. Thus, these results offered us a novel strategy to design and fabricate the phthalazinone-based microporous organic polymers with varied porosity.

Considering the special *N, O*-heteroatom structure, the relatively high surface areas and the microporous nature of PHCTFs, we were prompted to further explore their property of CO_2 capture and separation from other gases. Figure 5 shows the adsorption isotherms of CO_2 at 273 K and 298 K up to a pressure of 1 bar for PHCTFs, and the CO_2 uptakes displayed a rapid rise in the initial stage which may result from the favorable interaction between CO_2 molecule and the polymer skeleton[37]. According to the adsorption behavior curves of the porous networks, PHCTFs, the adsorbed CO_2 amount continually increased with the pressure, implying that the adsorption had not reached its equilibrium or saturated state in the investigated pressure range[38]. Among the PHCTs, PHCTF-1c exhibited the best performance on the adsorption of CO_2 reaching 17.1 wt% at 273 K and 1 bar, which may fall behind that of CPOP-1 and PPF-1 (up to 21.2[39] and 26.7 wt%[6] respectively), but is still comparable to other porous polymers, such as CMPs (4.0−17.0 wt%)[40], BLPs (7.4−12.8 wt%)[41] and POFs (12.2−18.0 wt%)[42]. Generally, pores less than 1.0 nm may be more effective towards CO_2 capture at low pressure since the molecular size of CO_2 is 0.36 nm[43]. However, PHCTF-1c still illustrated the highest CO_2 uptake for its dominant highest BET surface area among the resultant CTFs. Due to the high affinity of polymer skeleton toward CO_2 resulted from the naphthyridine containing abundant electron-rich nitrogen and oxygen atoms, PHCTF-1a, PHCTF-1b, PHCTF-2a and PHCTF-2b also possess satisfactory CO_2 uptakes at 273 K and 1 bar, up to 10.2, 9.4, 13.5 and 13.6 wt%, respectively. These uptakes may be inferior to materials such as FCTF-1-600 (24.3 w%)[44] and BILP-4 (23.5 wt%)[45], but still notably exceed or are competitive with a lot of organic porous organic polymer networks, such as PAF-3 (8 wt%)[15a], CMP-1 (9 wt%)[46], TBI-2 (11.8 wt%)[47]. The PHCTF-2 were constructed from THPZ-DN through the same polymerization process as PHCTF-1a and -1b, but exhibited the less BET surface areas in comparison to that of PHCTF-1a and -1b because of the less stereoscopic conformation. Nevertheless, it is noted that the higher CO_2 uptakes are obtained for PHCTF-2 with the relatively lower surface areas compared to PHCTF-1a and -1b. First of all, the narrow, uniform pore size distribution and smaller pore size less than 1 nm of PHCTF-2 resulted from the possible π-π stacking between layers may be one of the important factors. As we know, the narrow pore size distribution and small pore size play the same important roles compared to the high surface areas, sometimes even more through improved molecular interaction[28b] and the trapping-effect[48]. Another possibility can be attributed to their higher charge density at the sulfur site of networks (Table S1) that can facilitate local-dipole/quadrupole interactions with carbon dioxide[49]. Through the comparison and analysis of the adsorption performance to CO_2 of PHCTFs, it is apparent that the N, O and S atoms in PHCTFs create a high electric field on the network surface leading to a high binding force with quadrupolar CO_2 molecules[35]. Moreover, the further optimized conformation leads to the narrow, uniform pore size distribution, which contributes to improve the molecular

interaction between polar heteroatoms (N, O and S) and CO_2 molecules.

To understand and gain further insights from the host-guest interaction, Q_{st} (CO_2 isosteric enthalpies) of PHCTFs toward CO_2 were calculated from the CO_2 adsorption isotherms at 273 K and 298 K in term of Clausius-Clapeyron eqution[50]. Figure 6 shows the plots of the functions of adsorbed amount of CO_2 to isosteric enthalpies, and PHCTFs exhibited a relative high Q_{st}, approximate or even far exceed 30 kJ/mol, which are parallel to some reported heterocyclic rings-containing MOPs, such as CMPs (27.0-33.0 kJ/mol)[51] and COFs (15-30 kJ/mol)[52]. Though PHCTFs have high enthalpies on low adsorption capacities, the Q_{st} values decrease gradually with the increase of CO_2 adsorption, indicating the obvious adsorption behaviors of CO_2 molecule on the PHCTFs network skeleton rather than aggregate. PHCTF-2 have relative lower surface areas, however their higher CO_2 uptakes than that of PHCTF-1a and -1b might be partly attributed to the high values of heat of adsorption at high coverage, because of the introduction of polar S atom apart from N and O atoms in phthalazinone core. The highest CO_2 capacity refers to its high BET surface area, though PHCTF-1c shows the lowest isosteric heat. The virial plots of CO_2 for PHCTFs show quite good straight lines (Figure 6). The interaction between CO_2 molecule and pore surface of the polymers networks represents by the first virial coefficients, A_0, which are the intercepts of the lines. And according to A_0, we can calculate the Henry's law constants (K_H) through $K_H = \exp(A_0)$. Thus, the limiting enthalpy of adsorption (Q_0), which is the Q_{st} at zero surface CO_2 coverage, can be obtained from the plot slope of ln K_H versus 1/T. From the values at 273 and 298 K shown in Table 3, it can be seen that the A_0 and K_H values of PHCTF-2s exceed those of PHCTF-1s, the same as the Q_0.

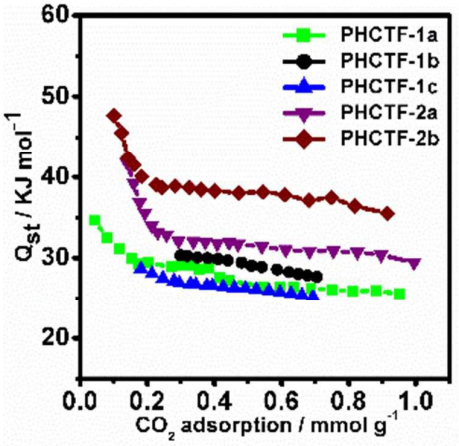

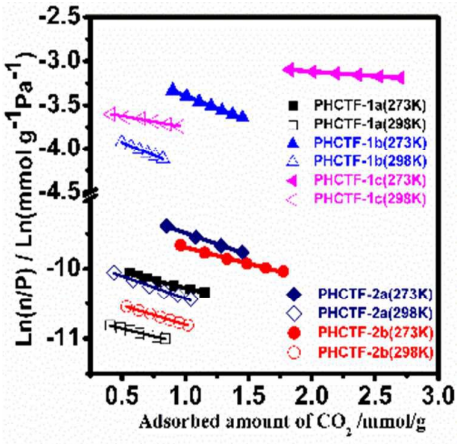

Figure 6. Variations of enthalpies of adsorption with the adsorbed amount of CO_2 (up) and virial plots (down) for PHCTFs.

Table 3. K_H, A_0, and Q_0 values of CO_2 adsorption in PHCTFs.

PHCTF	T (K)	K_H (mol g^{-1} Pa^{-1})	A_0 Ln (mol g^{-1} Pa^{-1})	Q_0 (kJ mol^{-1})
1a	273	5.43×10^{-5}	-9.820	22.2
	298	2.39×10^{-5}	-10.640	
1b	273	5.91×10^{-2}	-2.828	21.6
	298	2.66×10^{-2}	-3.628	
1c	273	5.48×10^{-2}	-2.904	16.0
	298	3.03×10^{-2}	-3.495	
2a	273	1.42×10^{-4}	-8.860	25.0
	298	5.64×10^{-5}	-9.783	
2b	273	9.78×10^{-5}	-9.233	27.6
	298	3.52×10^{-5}	-10.254	

As the presence of abundant N, O-heteroatoms of phthalazinone core, we suppose that the PHCTFs may possess the potential in gas separation. Besides the CO_2 adsorption capacity, the single component gas adsorption isotherms of CH_4 and N_2 at 273 K up to 1 bar were also measured. The ratios of the Henry law constants were calculated from the initial slopes of the single component gas adsorption isotherms in the low pressure range (Table 3). Then, the ratios were used to estimate the selective performance of the CO_2/CH_4 and CO_2/N_2. The adsorption isotherms of CO_2, N_2 and CH_4 at 273 K, 0-1 bar are shown in Figure 7. The uptakes of CO_2 in the adsorption isotherms exhibit considerably higher than N_2 and CH_4 in the whole pressure range. The selectivity factors of the CO_2/N_2 of these PHCTFs are up to 52 at 273K, comparable to zeolitic imidazole frameworks (ZIFs, 20-50)[53] and porous polymers, such as APOPs (23.8-43.4)[54] and BILPs (59−113)[45, 55]. For the adsorption and selectivity performance of PHCTFs, it can be found that PHCTF-2 simultaneously possesses relatively higher CO_2 uptakes and CO_2/N_2 selectively than PHCTF-1a and -1b. The higher CO_2 uptake can be derived from the introduction

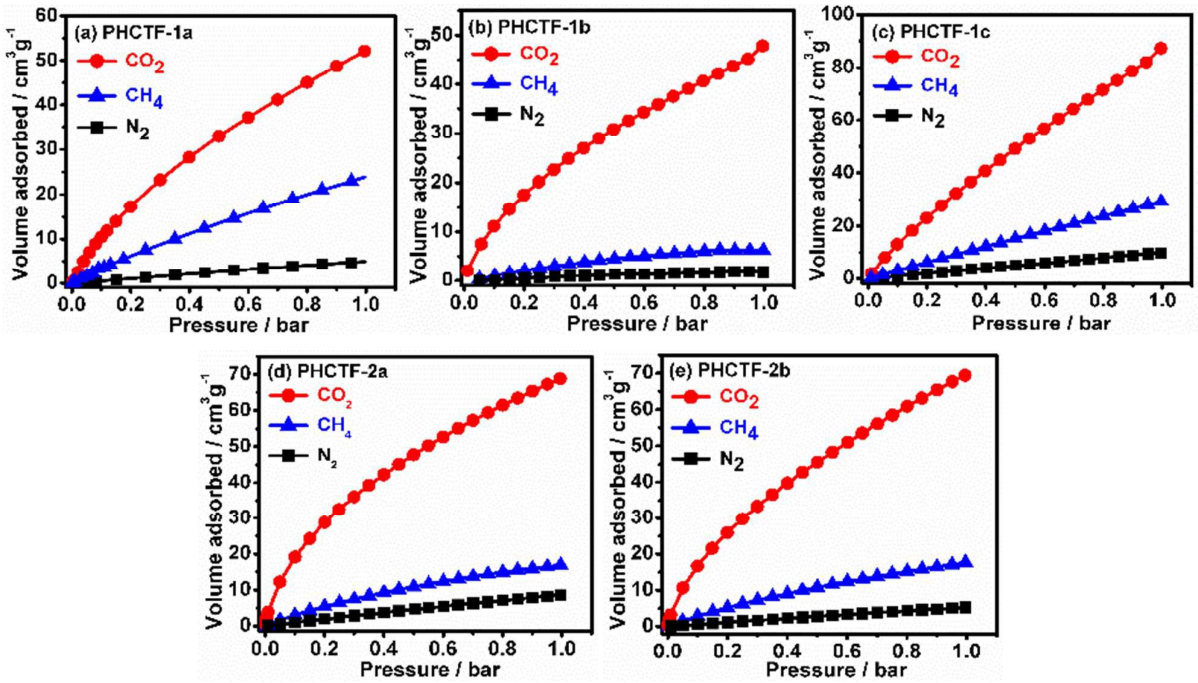

Figure 7. Adsorption isotherms of CO_2, CH_4 and N_2 gases at 273 K for PHCTFs.

polar S atom apart from N, O heteroatoms (Table S1). The narrow pore size distribution also leads to fine selectivity.Although PHCTF-1c exhibited the highest CO_2 uptake, however the more mesoporous area and the wider pore size distribution may be disadvantageous for the recognition of the small CO_2 (3.30 Å) from the large N_2 (3.64 Å) molecule which encumber its high CO_2 uptake simultaneously with excellent selectivity. However, PHCTFs exhibited the different adsorption behaviors toward CH_4 and N_2. Apparently, the higher uptake of CH_4 than N_2 for PHCTFs results from the higher critical temperature of CH_4 (191 K) than N_2 (126 K), because the gas solubility coefficient in a polymer is positively correlated with its critical temperature[56]. So, the selectivity of CO_2/CH_4 may be lower than that of CO_2/N_2 for PHCTFs, which is up to 12 and comparable to some microporous polymers[55a] and some ZIFs[53].

Hydrogen, with a large specific energy, is a kind of green fuel and suitable candidate to replace gasoline and other fossil fuels. In recent years, microporous organic polymers with high specific surface area, narrow pore distribution and electron-rich systems are of interest to be invaluable in the fields of gas storage, especially for the storage of hydrogen. So the hydrogen physisorption isotherms of PHCTFs were measured at 77 K and 1 bar, and are shown in Figure 8. Overall, for PHCTF-1c with the highest BET specific surface area, its hydrogen uptake is up to 1.92 wt% at 77 K and 1 bar, which is comparable to Trip(Me)-PIMs[57] (1.79 wt%, S_{BET} = 1760 m^2 g^{-1}) and P(Fe-TTPP)[58] (~1.5 wt%, SBET = 1248 m^2 g^{-1}) under the same condition. Also, this result is satisfactory and superior to some other MOPs with higher specific surface area, such as PPN-3[16a] (1.58 wt%, S_{BET} = 2840 m^2 g^{-1}), PAF-1[15b] (1.50 wt%, S_{BET} = 5600 m^2 g^{-1}) and COF-102[59] (1.2 wt%, S_{BET} = 3620 m^2 g^{-1}) at 77 K and 1 bar. These indicate that the rational design and selection of the building blocks are very important to afford excellent capacity of the hydrogen. On the one hand, the high specific surface area is very necessary. On the other hand, the molecular structure and chemical nature of the building blocks still play crucial roles[60].

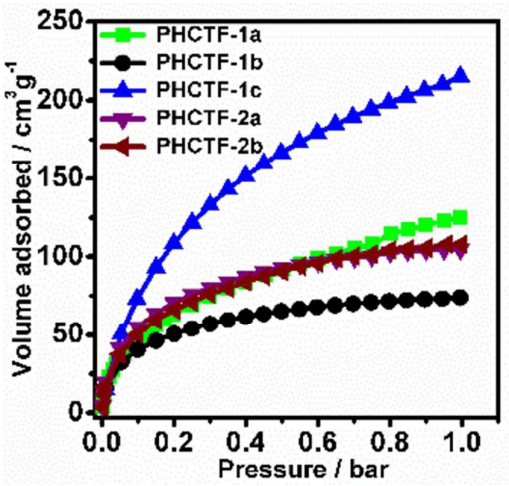

Figure 8. Hydrogen adsorption isotherms of the obtained PHCTFs at 77 K.

Table 4. Adsorption capacities and selectivity of PHCTFs.

Sample	CO_2 uptake [a] (wt %)		CO_2 selectivity (initial slope)		H_2 uptake [b] (wt %)
	273K	298K	CO_2/N_2	CO_2/CH_4	77K
PHCTF1a	10.2	6.2	22:1	4:1	1.12
PHCTF1b	9.4	6.0	49:1	9:1	0.66
PHCTF1c	17.1	10.0	12:1	4:1	1.92
PHCTF2a	13.5	8.6	38:1	12:1	0.93
PHCTF2b	13.6	7.2	52:1	11:1	0.96

[a] Uptakes for CO_2 at 1 bar; [b] Uptakes for H_2 at 1 bar.

Conclusions

The phthalazinone-based microporous organic polymer networks, PHCTFs, were constructed by ionothermal reaction with relatively high specific surface area and uniform pore size distribution. The chemical structures of PHCTFs have been well confirmed by FTIR and elemental analysis. The surface morphologies were evaluated by field-emission scanning electron microscopy (FE-SEM), and the local structure was observed through transmission electron microscopy (TEM). The measurements of sorption of nitrogen at 77 K showed that the polymers have large BET surface up to 1845 $m^2 g^{-1}$. Besides, their CO_2 adsorption capacities are up to 17.1 wt% (273 K/1 bar), and the polymers possess uptake of hydrogen (1.92 wt%, 77 K/1 bar). Also, PHCTFs exhibit good selectivity of CO_2/N_2 (52, 273 K/1 bar) and CO_2/CH_4 (12, 273 K/1 bar). These results indicate that the rigid, twisted and asymmetric phthalazinone structure can be used to construct satisfactory PHCTFs with good adsorption and separation properties. At the same time, the pore size distributions of the afforded PHCTFs can be adjusted through the change of the conformation of phthalazinone. The introduction of polar electron-rich S atom can further increase the CO_2 uptake of PHCTFs apart from abundant N, O heteroatoms of phthalazinone structure. These results indicate that the obtained the phthalazinone-based microporous organic polymer networks, PHCTFs, are promising functional materials for gas separation and storage.

Acknowledgements

The present research was financially supported by National Natural Science Foundation of China (No. 51473025) and Chinese Universities Scientific Fund (DUT13LK20). The authors acknowledge the High Performance Computing Centre of Dalian University of Technology for providing computational resources which have contributed to the research results.

Notes and references

1 K. S. Sing, Pure. *Appl. Chem.*, 1985, **57**, 603-619.
2 Y. Xu, S. Jin, H. Xu, A. Nagai and D. Jiang, *Chem. Soc. Rev.*, 2013, **42**, 8012-8031.
3 R. M. Barrer, *Zeolites*, 1981, **1**, 130-140.
4 Z. ALOthman, *Materials*, 2012, **5**, 2874-2902.
5 (a) S. Ma and H.-C. Zhou, *Chem. Commun.*, 2010, **46**, 44-53; (b) J.R.Long and O. M. Yaghi, *Chem. Soc. Rev.*, 2009, **38**, 1211214; (c) H. Li, M. Eddaoudi, M. O'Keeffe and O. M. Yaghi, *Nature*, 1999, **402**, 276-279.
6 Y. Zhu, H. Long and W. Zhang, *Chem. Mater.*, 2013, **25**, 1630-1635.
7 (a) J. Germain, J. M. J. Fréchet and F. Svec, *Small*, 2009, **5**, 1098-1111; (b) S. Xu, Y. Luo and B. Tan, *Macromol. Rapid. Comm.*, 2013, **34**, 471-484.
8 X. Zhang, J. Lu and J. Zhang, *Chem. Mater.*, 2014, **26**, 4023-4029.
9 (a) J. Y. Lee, C. D. Wood, D. Bradshaw, M. J. Rosseinsky and A. I. Cooper, *Chem. Commun.*, 2006, **25**, 2670-2672; (b) C. D. Wood, B. Tan, A. Trewin, F. Su, M. J. Rosseinsky, D. Bradshaw, Y. Sun, L. Zhou and A. I. Cooper, *Adv. Mater.*, 2008, **20**, 1916-1921.
10 H. B. Park, C. H. Jung, Y. M. Lee, A. J. Hill, S. J. Pas, S. T. Mudie, E. Van Wagner, B. D. Freeman and D. J. Cookson, *Science*, 2007, **318**, 254-258.
11 (a) X. Du, Y. Sun, B. Tan, Q. Teng, X. Yao, C. Su and W. Wang, *Chem. Commun.*, 2010, **46**, 970-972; (b) J. Schmidt, J. Weber, J. D. Epping, M. Antonietti and A. Thomas, *Adv. Mater.*, 2009, **21**, 702-705; (c) J. Luo, X. Zhang and J. Zhang, *ACS Catal.*, 2015, **5**, 2250-2254.
12 (a) Y. Wang, N. B. McKeown, K. J. Msayib, G. A. Turnbull and I. D. W. Samuel, *Sensors-Basel*, 2011, **11**, 2478-2487; (b) J. C. Thomas, J. E. Trend, N. A. Rakow, M. S. Wendland, R. J. Poirier and D. M. Paolucci, *Sensors-Basel*, 2011, **11**, 3267-3280.
13 (a) X. Feng, X. Ding and D. Jiang, *Chem. Soc. Rev.*, 2012, **41**, 6010-6022; (b) A. P. Cote, A. I. Benin, N. W. Ockwig, M. O'Keeffe, A. J. Matzger and O. M. Yaghi, *Science*, 2005, **310**, 1166-1170; (c) H. M. El-Kaderi, J. R. Hunt, J. L. Mendoza-Cortes, A. P. Cote, R. E. Taylor, M. O'Keeffe and O. M. Yaghi, *Science*, 2007, **316**, 268-272.
14 (a) F. Vilela, K. Zhang and M. Antonietti, *Energ. Environ. Sci.*, 2012, **5**, 7819-7832; (b) J. X. Jiang, F. Su, A. Trewin, C. D. Wood, N. L. Campbell, H. Niu, C. Dickinson, A. Y. Ganin, M. J. Rosseinsky, Y. Z. Khimyak and A. I. Cooper, *Angew. Chem. Int. Edit.*, 2007, **46**, 8574-8578.
15 (a) T. Ben, C. Pei, D. Zhang, J. Xu, F. Deng, X. Jing and S. Qiu, *Energ. Environ. Sci.*, 2011, **4**, 3991-3999; (b) T. Ben, H. Ren, S. Ma, D. Cao, J. Lan, X. Jing, W. Wang, J. Xu, F. Deng, J. M. Simmons, S. Qiu and G. Zhu, *Angew. Chem. Int. Edit.*, 2009, **48**, 9457-9460; (c) Y. Yuan, F. Sun, H. Ren, X. Jing, W. Wang, H. Ma, H. Zhao and G. Zhu, *J. Mater. Chem.*, 2011, **21**, 13498-13502.
16 (a) W. Lu, D. Yuan, D. Zhao, C. I. Schilling, O. Plietzsch, T. Muller, S. Bräse, J. Guenther, J. Blümel, R. Krishna, Z. Li and H.-C. Zhou, *Chem. Mater.*, 2010, **22**, 5964-5972; (b) D. Yuan, W. Lu, D. Zhao and H.-C. Zhou, *Adv. Mater.*, 2011, **23**, 3723-3725.
17 (a) P. M. Budd, B. S. Ghanem, S. Makhseed, N. B. McKeown, K. J. Msayib and C. E. Tattershall, *Chem. Commun.*, 2004, **2**, 230-231; (b) N. B. McKeown and P. M. Budd, *Chem. Soc. Rev.*, 2006, **35**, 675-683; (c) N. B. McKeown, B. Gahnem, K. J. Msayib, P. M. Budd, C. E. Tattershall, K. Mahmood, S. Tan, D. Book, H. W. Langmi and A. Walton, *Angew. Chem. Int. Edit.*, 2006, **45**, 1804-1807.

18 (a) J. Germain, J. Hradil, J. M. J. Fréchet and F. Svec, *Chem. Mater.*, 2006, **18**, 4430-4435; (b) M. P. Tsyurupa and V. A. Davankov, *React. Funct. Polym.*, 2006, **66**, 768-779; (c) C. D. Wood, B. Tan, A. Trewin, H. Niu, D. Bradshaw, M. J. Rosseinsky, Y. Z. Khimyak, N. L. Campbell, R. Kirk, E. Stöckel and A. I. Cooper, *Chem. Mater.*, 2007, **19**, 2034-2048; (d) O. W. Webster, F. P. Gentry, R. D. Farlee and B. E. Smart, *Macromol. Symp.*, 1992, **54**, 477-482.

19 (a) M. Rose, W. Bohlmann, M. Sabo and S. Kaskel, *Chem. Commun.*, 2008, **21**, 2462-2464; (b) S. Yuan, S. Kirklin, B. Dorney, D.-J. Liu and L. Yu, *Macromolecules*, 2009, **42**, 1554-1559; (c) O. K. Farha, A. M. Spokoyny, B. G. Hauser, Y.-S. Bae, S. E. Brown, R. Q. Snurr, C. A. Mirkin and J. T. Hupp, *Chem. Mater.*, 2009, **21**, 3033-3035; (d) F. J. Uribe-Romo, J. R. Hunt, H. Furukawa, C. Klöck, M. O'Keeffe and O. M. Yaghi, *J. Am. Chem. Soc.*, 2009, **131**, 4570-4571.

20 (a) T. Tozawa, J. T. Jones, S. I. Swamy, S. Jiang, D. J. Adams, S. Shakespeare, R. Clowes, D. Bradshaw, T. Hasell, S. Y. Chong, C. Tang, S. Thompson, J. Parker, A. Trewin, J. Bacsa, A. M. Slawin, A. Steiner and A. I. Cooper, *Nat. Mater.*, 2009, **8**, 973-978; (b) Y. Jin, B. A. Voss, R. McCaffrey, C. T. Baggett, R. D. Noble and W. Zhang, *Chem. Sci.*, 2012, **3**, 874-877.

21 A. P. Cote, H. M. El-Kaderi, H. Furukawa, J. R. Hunt and O. M. Yaghi, *J. Am. Chem. Soc.*, 2007, **129**, 12914-12915.

22 P. Pandey, A. P. Katsoulidis, I. Eryazici, Y. Wu, M. G. Kanatzidis and S. T. Nguyen, *Chem. Mater.*, 2010, **22**, 4974-4979.

23 (a) P. Kuhn, A. Thomas and M. Antonietti, *Macromolecules*, 2009, **42**, 319-326; (b) P. Kuhn, A. Forget, J. Hartmann, A. Thomas and M. Antonietti, *Adv. Mater.*, 2009, **21**, 897-901; (c) P. Kuhn, A. Forget, D. Su, A. Thomas and M. Antonietti, *J. Am. Chem. Soc.*, 2008, **130**, 13333-13337; (d) P. Kuhn, M. Antonietti and A. Thomas, *Angew. Chem. Int. Edit.*, 2008, **47**, 3450-3453.

24 Y. P. Tang, H. Wang and T. S. Chung, *Chemsuschem*, 2015, **8**, 138-147.

25 X. Zhu, C. Tian, S. M. Mahurin, S. H. Chai, C. Wang, S. Brown, G. M. Veith, H. Luo, H. Liu and S. Dai, *J. Am. Chem. Soc.*, 2012, **134**, 10478-10484.

26 A. Bhunia, I. Boldog, A. Möller and C. Janiak, *J. Mater. Chem. A*, 2013, **1**, 14990-14999.

27 S. Hug, M. E. Tauchert, S. Li, U. E. Pachmayr and B. V. Lotsch, *J. Mater. Chem.*, 2012, **22**, 13956-13964.

28 (a) Y. Liu, S. Wu, G. Wang, G. Yu, J. Guan, C. Pan and Z. Wang, *J. Mater. Chem. A*, 2014, **2**, 7795-7801; (b) Q. Chen, M. Luo, P. Hammershoj, D. Zhou, Y. Han, B. W. Laursen, C. G. Yan and B. H. Han, *J. Am. Chem. Soc.*, 2012, **134**, 6084-6087; (c) H. Lim, M. C. Cha and J. Y. Chang, *Macromol. Chem. Phys.*, 2012, **213**, 1385-1390.

29 (a) G. Yu, C. Liu, J. Wang, J. Xu and X. Jian, *Polym. Int.*, 2010, **59**, 1233-1239; (b) G. Yu, C. Liu, J. Wang, G. Li, Y. Han and X. Jian, *Polymer*, 2010, **51**, 100-109; (c) G. Yu, J. Wang, C. Liu, E. Lin and X. Jian, *Polymer*, 2009, **50**, 1700-1708; (d) G. Yu, C. Liu, H. Zhou, J. Wang, E. Lin and X. Jian, *Polymer*, 2009, **50**, 4520-4528.

30 S. Yoshida and A. S. Hay, *Macromolecules*, 1995, **28**, 2579-2581.

31 Q. Liang, P. Liu, C. Liu, X. Jian, D. Hong and Y. Li, *Polymer*, 2005, **46**, 6258-6265.

32 J. Y. Wang, G. X. Liao, C. Liu and X. G. Jian, *J. Polym. Sci. Pol. Chem.*, 2004, **42**, 6089-6097.

33 S. A. Weissman, D. Zewge and C. Chen, *J. Org. Chem.*, 2005, **70**, 1508-1510.

34 A. Bhunia, V. Vasylyeva and C. Janiak, *Chem. Commun.*, 2013, **49**, 3961-3963.

35 S. Wu, Y. Liu, G. Yu, J. Guan, C. Pan, Y. Du, X. Xiong and Z. Wang, *Macromolecules*, 2014, **47**, 2875-2882.

36 Y. C. Zhao, L. M. Zhang, T. Wang and B. H. Han, *Polym. Chem.*, 2014, **5**, 614-621.

37 G. Li and Z. Wang, *Macromolecules*, 2013, **46**, 3058-3066.

38 Y. Yang, Q. Zhang, S. Zhang and S. Li, *Polymer*, 2013, **54**, 5698-5702.

39 Q. Chen, M. Luo, P. Hammershøj, D. Zhou, Y. Han, B. W. Laursen, C.-G. Yan and B.-H. Han, *J. Am. Chem. Soc.*, 2012, **134**, 6084-6087.

40 (a) A. Thomas, Angewandte Chemie, 2010, 49, 8328-8344; (b) A. I. Cooper, *Adv. Mater.*, 2009, **21**, 1291-1295.

41 (a) K. T. Jackson, M. G. Rabbani, T. E. Reich and H. M. El-Kaderi, *Polym. Chem.*, 2011, **2**, 2775-2777; (b) T. E. Reich, S. Behera, K. T. Jackson, P. Jena and H. M. El-Kaderi, *J. Mater. Chem.*, 2012, **22**, 13524-13528.

42 A. P. Katsoulidis and M. G. Kanatzidis, *Chem. Mater.*, 2011, **23**, 1818-1824.

43 D. Cazorla-Amorós, J. Alcañiz-Monge and A. Linares-Solano, *Langmuir*, 1996, **12**, 2820-2824.

44 Y. Zhao, K. X. Yao, B. Teng, T. Zhang and Y. Han, *Energ. Environ. Sci.*, 2013, **6**, 3684-3692.

45 M. G. Rabbani and H. M. El-Kaderi, *Chem. Mater.*, 2012, **24**, 1511-1517.

46 J. X. Jiang, F. Su, A. Trewin, C. D. Wood, H. Niu, J. T. A. Jones, Y. Z. Khimyak and A. I. Cooper, *J. Am. Chem. Soc.*, 2008, **130**, 7710-7720.

47 Y. C. Zhao, Q. Y. Cheng, D. Zhou, T. Wang and B.-H. Han, *J. Mater. Chem.*, 2012, **22**, 11509-11514.

48 J. Germain, F. Svec and J. M. J. Fréchet, *Chem. Mater.*, 2008, **20**, 7069-7076.

49 M. Y. Jiang, Q. Wang, Q. Chen, X. M. Hu, X.-L. Ren, Z. H. Li and B. H. Han, *Polymer*, 2013, **54**, 2952-2957.

50 V. Krungleviciute, L. Heroux, A. D. Migone, C. T. Kingston and B. Simard, *J. Phys. Chem. B*, 2005, **109**, 9317-9320.

51 R. Dawson, D. J. Adams and A. I. Cooper, *Chem. Sci.*, 2011, **2**, 1173-1177.

52 S. Y. Ding and W. Wang, *Chem. Soc. Rev.*, 2013, **42**, 548-568.

53 R. Banerjee, H. Furukawa, D. Britt, C. Knobler, M. O'Keeffe and O. M. Yaghi, *J. Am. Chem. Soc.*, 2009, **131**, 3875-3877.

54 W. C. Song, X. K. Xu, Q. Chen, Z. Z. Zhuang and X. H. Bu, *Polym. Chem.*, 2013, **4**, 4690-4696.

55 (a) M. G. Rabbani and H. M. El-Kaderi, *Chem. Mater.*, 2011, **23**, 1650-1653; (b) M. G. Rabba, T. E. Reich and H. M. El-Kaderi, *Abstr Pap Am Chem S*, 2012, **243**, 1156.

56 V. M. Shah, B. J. Hardy and S. A. Stern, *J. Polym. Sci. Pol. Phys.*, 1993, **31**, 1185-1185.

57 B. S. Ghanem, M. Hashem, K. D. M. Harris, K. J. Msayib, M. Xu, P. M. Budd, N. Chaukura, D. Book, S. Tedds, A. Walton and N. B. McKeown, *Macromolecules*, 2010, **43**, 5287-5294.

58 J. Xia, S. Yuan, Z. Wang, S. Kirklin, B. Dorney, D. J. Liu and L. Yu, *Macromolecules*, 2010, **43**, 3325-3330.
59 H. Furukawa and O. M. Yaghi, *J. Am. Chem. Soc.*, 2009, **131**, 8875-8883.
60 Q. Chen, J. X. Wang, Q. Wang, N. Bian, Z. H. Li, C.G. Yan and B. H. Han, *Macromolecules*, 2011, **44**, 7987-7993.

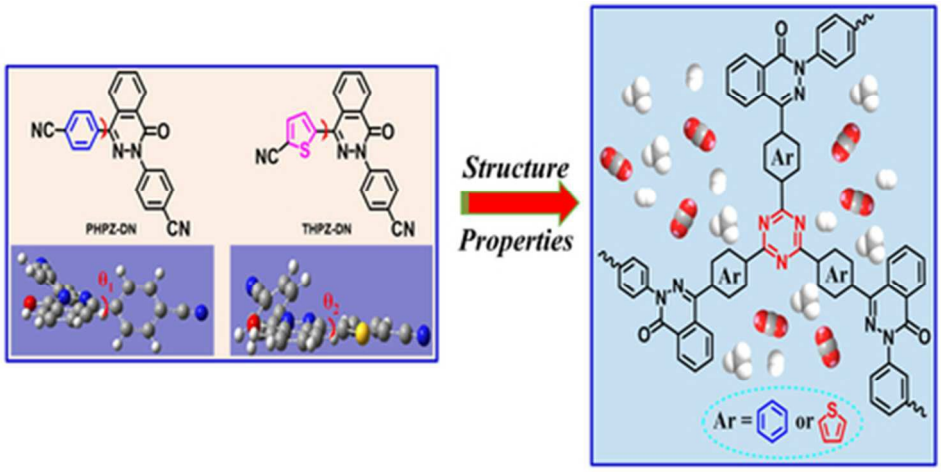

39x19mm (300 x 300 DPI)